International Journal of
Molecular Sciences

MDPI

Article

Antibacterial and Cellular Behaviors of Novel Zinc-Doped Hydroxyapatite/Graphene Nanocomposite for Bone Tissue Engineering

H. Maleki-Ghaleh [1], M. H. Siadati [2], A. Fallah [3,4], B. Koc [3,4], M. Kavanlouei [5], P. Khademi-Azandehi [6], E. Moradpur-Tari [7], Y. Omidi [8], J. Barar [1,9], Y. Beygi-Khosrowshahi [10], Alan P. Kumar [11,12,*] and Kh. Adibkia [1,9,*]

1 Research Center for Pharmaceutical Nanotechnology, Biomedicine Institute, Tabriz University of Medical Sciences, Tabriz 51664-14766, Iran; h_maleki@sut.ac.ir (H.M.-G.); jbarar@tbzmed.ac.ir (J.B.)
2 Faculty of Materials Science and Engineering, K. N. Toosi University of Technology, Tehran 19919-43344, Iran; siadati@kntu.ac.ir
3 Faculty of Engineering and Natural Sciences, Sabanci University, Istanbul 34956, Turkey; ali.fallah@sabanciuniv.edu (A.F.); bahattin.koc@sabanciuniv.edu (B.K.)
4 Nanotechnology Research and Application Center (SUNUM), Sabanci University, Istanbul 34956, Turkey
5 Materials Engineering Department, Faculty of Engineering, Urmia University, Urmia 57561-51818, Iran; m.kavanlouei@urmia.ac.ir
6 Research Center for Advanced Materials, Faculty of Materials Engineering, Sahand University of Technology, Tabriz 51335-1996, Iran; p_khademi@hotmail.com
7 Materials Engineering Department, Faculty of Engineering, Tarbiat Modares University, Tehran 14115-111, Iran; e.moradpour@modares.ac.ir
8 Department of Pharmaceutical Sciences, College of Pharmacy, Nova Southeastern University, Fort Lauderdale, FL 33314, USA; yomidi@nova.edu
9 Department of Pharmaceutics, Faculty of Pharmacy, Tabriz University of Medical Sciences, Tabriz 51664-14766, Iran
10 Department of Chemical Engineering, Faculty of Engineering, Azarbaijan Shahid Madani University, Tabriz 53751-71379, Iran; yonesbeygi@gmail.com
11 Department of Pharmacology, Yong Loo Lin School of Medicine, National University of Singapore, Singapore 117599, Singapore
12 NUS Centre for Cancer Research, Yong Loo Lin School of Medicine, National University of Singapore, Singapore 117597, Singapore
* Correspondence: apkumar@nus.edu.sg (A.P.K.); adibkia@tbzmed.ac.ir (K.A.); Tel.: +65-65165456 (A.P.K.); +98-4133372250 (K.A.)

Abstract: Bacteria are one of the significant causes of infection in the body after scaffold implantation. Effective use of nanotechnology to overcome this problem is an exciting and practical solution. Nanoparticles can cause bacterial degradation by the electrostatic interaction with receptors and cell walls. Simultaneously, the incorporation of antibacterial materials such as zinc and graphene in nanoparticles can further enhance bacterial degradation. In the present study, zinc-doped hydroxyapatite/graphene was synthesized and characterized as a nanocomposite material possessing both antibacterial and bioactive properties for bone tissue engineering. After synthesizing the zinc-doped hydroxyapatite nanoparticles using a mechanochemical process, they were composited with reduced graphene oxide. The nanoparticles and nanocomposite samples were extensively investigated by transmission electron microscopy, X-ray diffraction, and Raman spectroscopy. Their antibacterial behaviors against Escherichia coli and Staphylococcus aureus were studied. The antibacterial properties of hydroxyapatite nanoparticles were found to be improved more than 2.7 and 3.4 times after zinc doping and further compositing with graphene, respectively. In vitro cell assessment was investigated by a cell viability test and alkaline phosphatase activity using mesenchymal stem cells, and the results showed that hydroxyapatite nanoparticles in the culture medium, in addition to non-toxicity, led to enhanced proliferation of bone marrow stem cells. Furthermore, zinc doping in combination with graphene significantly increased alkaline phosphatase activity and proliferation of mesenchymal stem cells. The antibacterial activity along with cell biocompatibility/bioactivity of

check for updates

Citation: Maleki-Ghaleh, H.; Siadati, M.H.; Fallah, A.; Koc, B.; Kavanlouei, M.; Khademi-Azandehi, P.; Moradpur-Tari, E.; Omidi, Y.; Barar, J.; Beygi-Khosrowshahi, Y.; et al. Antibacterial and Cellular Behaviors of Novel Zinc-Doped Hydroxyapatite/Graphene Nanocomposite for Bone Tissue Engineering. *Int. J. Mol. Sci.* **2021**, *22*, 9564. https://doi.org/10.3390/ijms22179564

Academic Editors: Francesco Trotta, Fabrizio Caldera and Ali Zarrabi

Received: 21 July 2021
Accepted: 29 August 2021
Published: 3 September 2021

Publisher's Note: MDPI stays neutral with regard to jurisdictional claims in published maps and institutional affiliations.

zinc-doped hydroxyapatite/graphene nanocomposite are the highly desirable and suitable biological properties for bone tissue engineering successfully achieved in this work.

Keywords: antibacterial; biocompatibility; nanocomposite; hydroxyapatite; zinc; graphene

1. Introduction

Bacterial infections caused by orthopedic surgeries (such as implantation of bone scaffold and artificial joints) can lead to allergies, inflammation, and necrosis of tissues in the implanted area [1,2]. Damage in tissues could even require re-surgeries to remove the implant or scaffolds [3,4]. Using innovative materials to construct implants or bone scaffolds possessing antibacterial properties together with biocompatibility is an attractive solution to control bacterial infections [4,5]. Considering the biomaterials used for bone implants and scaffolds, hydroxyapatite (HA) is one of the preferred choices [6,7]. Possessing chemical composition of $Ca_{10}(PO_4)_6(OH)_2$, HA is one of the main components of bone (nearly 70%) which forms the mineral part of bones tissues [8]. Because HA is biocompatible, nontoxic, and non-inflammatory at the same time, it is one of the most favored biomaterials for fabricating bone scaffolds [9,10]. Due to its osteoinductivity and osteoconductivity properties, HA in scaffolds can accelerate new bone tissue formation [11]. As a significant factor in advancing the medical engineering field, nanotechnology can create superior capabilities in biomaterials by modifying their structures [12,13]. For example, upon modifying the crystal structure of HA by doping with antibacterial elements, and further compositing it with carbon nanomaterials, can not only improve the new HA nanocomposite material's bioactivity but also its other biological features such as antibacterial properties [14,15]. Zinc (Zn) has a unique state among the elements that have antibacterial properties [16]. Zn causes bacterial death due to mechanisms such as reactive oxygen species, such as peroxides and hydroxides, and direct reactions with bacterial proteins such as phospholipids [16,17]. Therefore, Zn as a doping element promotes HA nanoparticles' antibacterial potency while increasing its bioactivity [17]. Recent studies showed that Zn can boost osteoblast cell proliferation and osteogenic differentiation [18,19]. During the natural bone remodeling process, Zn is released from the bone. Research has shown that Zn released from bone reduces osteoclast resorption and increases osteoblast ossification [20]. Zn also accelerates the hydrolysis of phosphomonoesters to mineral phosphates, creating a suitable alkaline environment for mineral phosphate mineralization on the extracellular matrix (ECM) [21]. Moreover, Zn affects mitochondrial anaplerotic reactions by decreasing lactate, and increasing intermediates of the Krebs cycle; these increase citrate accumulation and deposition of bone apatite. As a result, due to increased citrate anabolism, mineralization occurs more rapidly [22]. The bioenergetic changes of mitochondria and transportation of calcium and citrate in the mitochondria and cytoplasm are manifest during stem cell differentiation [23]. Meanwhile, genes related to mitochondrial biogenesis, such as ERRα and PGC-1α, are activated to increase anaplerotic reactions to intermediate replenishment of the Krebs cycle [24]. As a result, it causes compounds such as α-ketoglutarate to have high concentrations during osteogenic differentiation. In addition, glutaminolysis-related genes such as GLAST, GLS, and GDH are also activated to produce more α-ketoglutarate. More expression of CS and CTP genes during differentiation helps increase citrate anabolism and citrate transportation, leading to citrate catabolism reduction [22]. The cooperation of Zn with Runx2 and OSX results in the Zn-Runx2/OSX-ZIP1 regulatory axis formation, increasing Zn transporter protein expression (ZIP1). An increase in ZIP1 leads to an influx of Zn into the cell, enhancing the proliferation and differentiation signaling pathways such as TGF-β and BMP. Since extracellular citrate deposition is derived from the metabolism of the mitochondrial Krebs cycle [25], induction of ZIP1 can reduce citrate catabolism by suppressing mitochondrial aconitase activity. Citrate catabolism reduction results in enhanced citrate accumulation and deposition, a crucial factor in bone-strengthening [26].

Meanwhile, graphene-based nanomaterials, due to their unique physical and chemical properties, have exceptional potential for use in biomedicine, such as drug delivery, cancer therapy, and tissue engineering [27,28]. For example, in bone tissue engineering, reduced graphene oxide (rGO) provides significant biological performance, such as improving osteoblastic differentiation and antibacterial activity [29,30]. Recent research work proved that graphene nanomaterials can not only deactivate bacteria with impressive results, but at the same time it has shown high osteoconductivity and osteoinductivity capacities for regulating osteogenic differentiation [31,32]. Moreover, graphene supports bone cell growth and osteogenic differentiation due to its high stiffness modulus and is suitable for bone scaffolds [33]. By integration of graphene and Zn-doped HA in the form of a nanocomposite, the synergistic effect of nanomaterial can be expected simultaneously to show two behaviors: antibacterial and bioactivity. In this study, Zn-doped HA nanoparticles were synthesized using a mechanochemical process, and rGO was composited to them by photochemical reduction to form a novel HA-based nanocomposite. The nanoparticles were characterized by transmission electron microscopy (TEM), X-ray diffraction (XRD), and Raman spectroscopy, and evaluation of their cellular behavior was conducted using mesenchymal stem cells (MSCs) by cell viability tests and alkaline phosphatase (ALP) activity. The antibacterial behaviors of nanoparticles were also studied with Escherichia coli (*E. coli*) and Staphylococcus aureus (*S. aureus*).

2. Results

2.1. Characterization of Nanoparticles

The X-ray photoelectron spectroscopy (XPS), XRD, and attenuated total reflectance-Fourier transform infrared (ATR-FTIR) characterizations of the nanoparticles have been thoroughly studied in the previous work [34]. The TEM images for (a) HA, (b) ZnHA, and (c) ZnHA-rGO nanoparticles are presented in Figure 1. As shown in Figure 1a,b, the HA and ZnHA nanoparticles have a flake-like or quasi-spherical shape with a rough surface. Figure 1c demonstrates the ZnHA-rGO sample; the ZnHA nanoparticles formed a nanocomposite with the rGO sheets. Furthermore, the phase analysis results (XRD patterns) in Figure 2 show the hexagonal structure for HA nanoparticles (JCPDS 09-432). The ZnHA nanoparticles also show a hexagonal structure like HA [35–38]. At the same time, compositing the ZnHA nanoparticles with rGO nanosheets did not affect the crystal structure, but a new peak associated with graphene nanosheets (002) appeared [39].

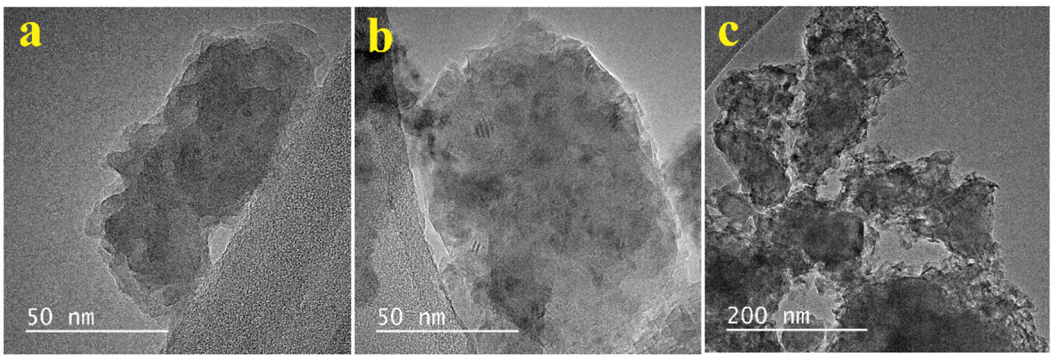

Figure 1. TEM images of (**a**) HA, and (**b**) ZnHA nanoparticles showing flake-like morphology, and (**c**) ZnHA-rGO showing ZnHA nanoparticles composited with rGO sheets.

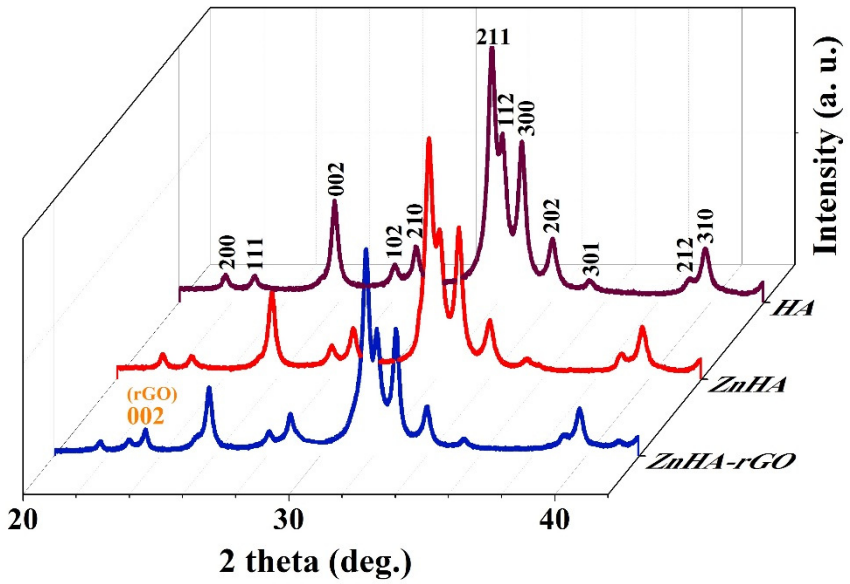

Figure 2. XRD patterns of HA, ZnHA, and ZnHA-rGO nanoparticles. The diffraction pattern of HA nanoparticles was well in accordance with the standard pattern of HA (JCPDS card No. 09–0432); hexagonal structure. The XRD patterns of ZnHA and ZnHA-rGO nanoparticles were highly similar to that of HA nanoparticles. A peak corresponding to graphene nanosheets (002) was seen in ZnHA-rGO.

Figure 3a shows the Raman spectra for HA, ZnHA, and ZnHA-rGO nanoparticles. Representative bands of the HA sample are associated with the doubly degenerate bending mode $v_2(PO_4^{3-})$ (426 cm^{-1}), triply degenerate bending mode $v_4(PO_4^{3-})$ (583 cm^{-1}), symmetric stretching mode $v_1(PO_4^{3-})$ (951 cm^{-1}), and asymmetric stretching mode $v_3(PO_4^{3-})$ (1024 cm^{-1}) [40–42]. These bands are also well-observed in the ZnHA and ZnHA-rGO spectra, indicating the stability of the molecular structure of HA after doping and compositing with Zn and rGO, respectively. In the ZnHA-rGO sample, two broad bands are related with the vibration of carbon atoms in the graphene lattice, the D and G bands in the range of 1347 and 1601 cm^{-1}, respectively [43]. The D band is associated with lattice distortions, and the G band is related to sp^2 hybridized carbon–carbon bonds in graphene [43]. Furthermore, Zn doping in the HA structure and its compositing with rGO has made PO_4^{3-} bands lower and broader. This is well seen in Figure 3b for the $v_1(PO_4^{3-})$ band in the region of 950 cm^{-1}. The difference in ionic radius between Zn^{2+} and Ca^{2+} can distort the PO_4^{3-} structure [40,41]. Moreover, the interaction between the rGO atoms with the surface atoms of HA nanoparticles can affect the structure of PO_4^{3-} [34].

2.2. In-Vitro Cell Analysis

The effect of nanoparticles on MSC proliferation was investigated for 7 and 14 days by MTT (3-(4,5-dimethylthiazol-2-yl)-2,5-diphenyltetrazolium bromide, a tetrazole) assay. As shown in Figure 4, the MSC proliferation in culture media treated by the nanoparticles is higher than in the control one. Moreover, doping HA nanoparticles with Zn increased MSC proliferation, and it was further enhanced by the addition of rGO.

ALP plays a vital function in the matrix mineralization process during bone formation. The bone differentiation capacity of MSCs was assessed by ALP activity after 7 and 14 days of incubation. The ALP activity in culture media treated with HA, ZnHA, and ZnHA-rGO nanoparticles compared with the control media is presented in Figure 5. The ALP activity of all three nanoparticles increased with incubation time, considerably higher for ZnHA-rGO.

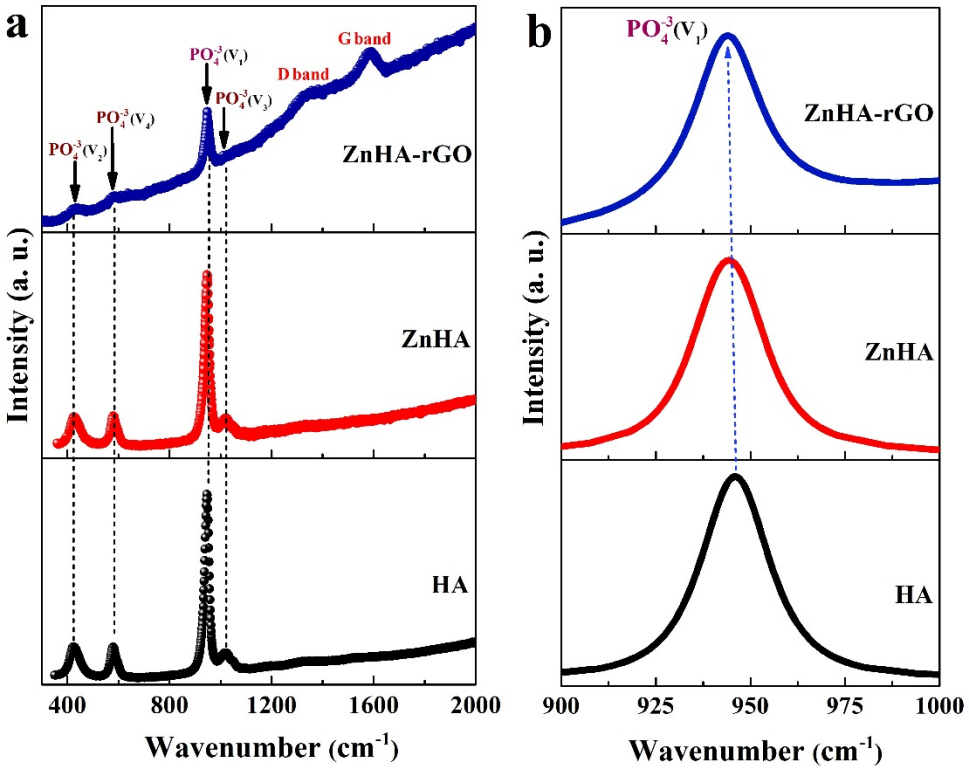

Figure 3. (**a**) Raman spectra of HA, ZnHA, and ZnHA-rGO nanoparticles, (**b**) Raman spectra in 900–1000 cm^{-1} range. Raman spectra indicate that the rGO nanosheets wrap the surface of ZnHA nanoparticles. Zn doping in the HA structure and its compositing with rGO has made PO_4^{3-} bands lower and broader.

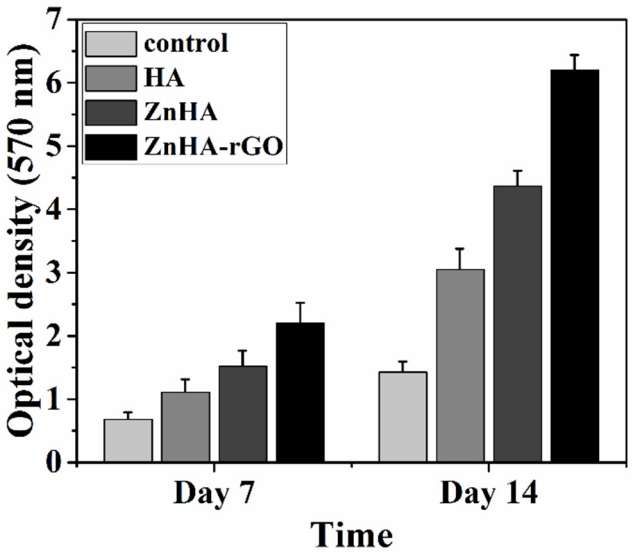

Figure 4. The viability of MSCs incubated in culture media treated by the HA, ZnHA, and ZnHA-rGO nanoparticles using MTT assay. During the incubation period (14 days), the presence of nanoparticles caused an appreciable increase in cell proliferation, especially ZnHA-rGO, compared to the non-treated control.

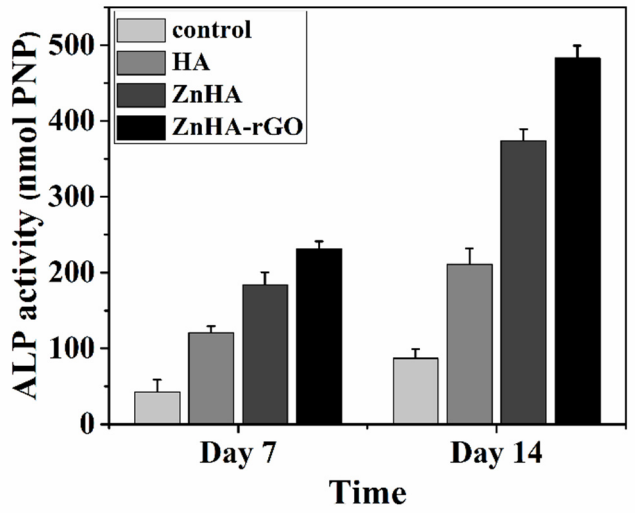

Figure 5. ALP activity of MSCs in culture media treated by the HA, ZnHA, and ZnHA-rGO nanoparticles. Incubation with ZnHA-rGO nanoparticles for 7 to 14 days significantly induced ALP activity.

2.3. Antibacterial Assay

Figure 6 shows the time-dependent cell viability for *E. coli* and *S. aureus* bacteria for HA, ZnHA, and ZnHA-rGO nanoparticles. The loss of viability of bacterial cells was assessed by the colony counting method after every 4 h interval. As shown in Figure 6, doping Zn in HA nanoparticles significantly affected the bacterial cell loss, and the inclusion of rGO increased it further.

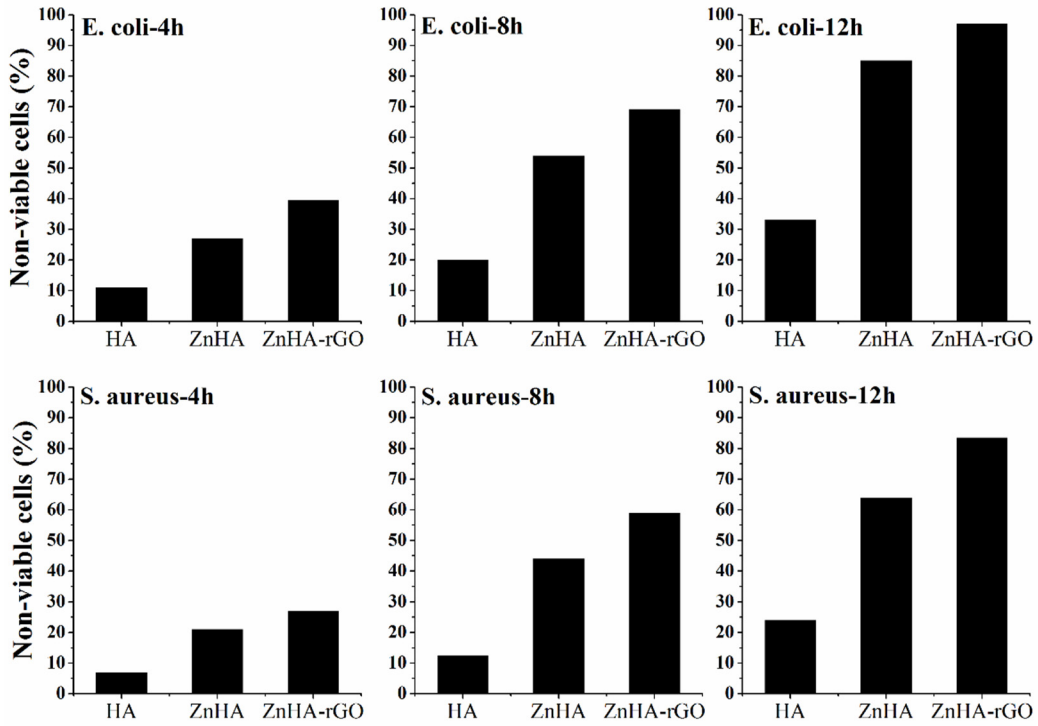

Figure 6. The loss of viability of *E. coli* and *S. aureus* bacteria after incubation with 100 μg mL^{-1} concentration of HA, ZnHA, and ZnHA-rGO nanoparticles for different time exposure (4, 8, and 12 h).

Figure 7 shows the disk diffusion antibacterial test results for all three nanoparticles. The inhibition zone indicates the resistance of nanoparticles against bacterial strains. The HA sample had a small inhibition zone against *E. coli* and *S. aureus*. Doping Zn in HA and compositing it with rGO showed significant impacts on the inhibition zone. Zn in HA

effectively inhibits the growth of *E. coli* and *S. aureus* on agars. The bactericidal activity of ZnHA nanoparticles can be due to the release of Zn ions, acting as an anti-bactericidal agent. Moreover, rGO further enhanced the antibacterial activity of ZnHA; a larger inhibition zone against bacteria. At the same time, the Gram-positive *S. aureus* was more resistant than Gram-negative *E. coli* for all samples.

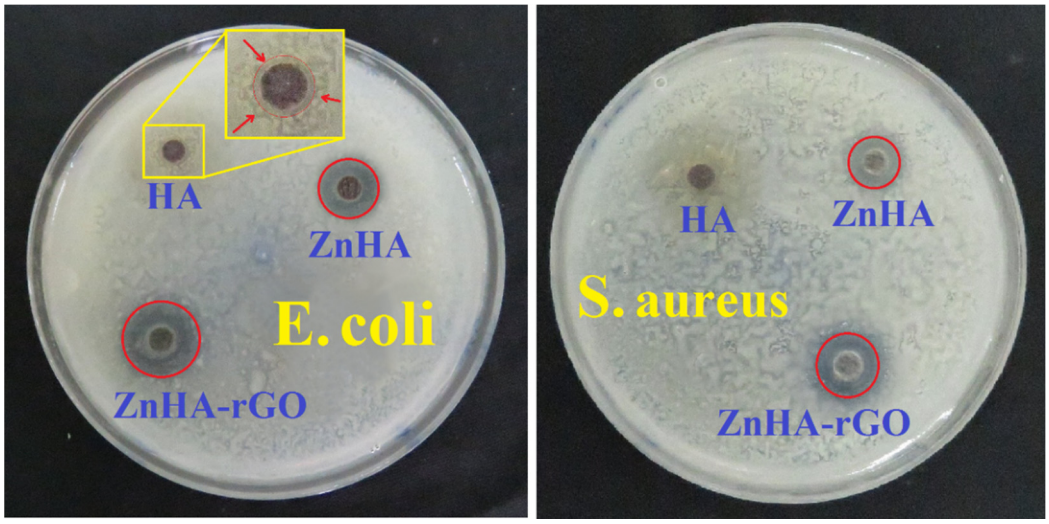

Figure 7. Disk diffusion tests for the evaluation of antibacterial activity of HA, ZnHA, and ZnHA-rGO nanoparticles against the *E. coli* and *S. aureus* strains. The zone of inhibition is highlighted with a red circle indicating a noticeable antibacterial effect.

3. Discussion

3.1. Cellular Behavior

Calcium ions in HA positively affect MSC proliferation in culture media [44]. The doped Zn in HA further promoted this phenomenon by stimulating signaling pathways that lead to boosting cell proliferation [18,19]. Simultaneous Zn doping and rGO compositing improved the adsorption of molecules on the surface of nanoparticles. It has been reported that rGO facilitates the adsorption of ions and proteins at the surface of nanoparticles [29,30], leading to improvement in cell proliferation [44].

The ALP enzyme participates in the process of maturation of osteoblast cells and alkalizes the environment, which results in hydrolyzing the phosphomonoesters to inorganic phosphates [45]. Mineralization of the organic phosphates results in the formation of ECM for the bone cells [46]. The presence of calcium, Zn ions, and rGO nanoparticles in the cell culture media can boost the activity of ALP enzymes, and as such, the differentiation of MSCs into osteoblasts would intensify [18,30].

3.1.1. Effect of Hydroxyapatite on Cellular Behavior

HA can differentiate and proliferate HMSCs by stimulating intracellular signaling. Stimulation of HMSCs by HA raises the activity of the CREB transcription factor, which regulates several osteoblast marker genes. HA nanoparticles can enter the cytoplasm through the endosome and decompose into its ingredients, calcium, and phosphate [47]. Xu et al. [47] revealed that increasing the intracellular concentration of calcium ions stimulates several signaling pathways, including calcium, cAMP, Ras, Rap1, and MAPK. As a product of adenylate cyclase activity, cAMP is a secondary messenger that arouses Epac and subsequently Rap1 [48]. Rap1 has the potential to activate Raf1, and Raf1 induces phosphorylation of MEK and ERK1/2, and Raf1 also activates PI3K and then AKT, which eventually increases the CREB transcription factor [49]. Phosphorylated CREB can help mRNA expression associated with osteoblastic differentiation, such as Runx2, ALP, OCN, Col1, and OSX [50].

3.1.2. Effect of Zinc on Cellular Behavior

Zn has been known as a stimulant factor of osteoblastic differentiation and proliferation in vitro and in vivo [51]. Several mechanisms have been identified for Zn-related osteogenesis, including several intracellular signaling pathways that eventually lead to the expression of genes that contribute to differentiation, mineralization, and proliferation. The mRNA and protein levels of the transcription factor Runx2, TGF-β, smad2, smad3, and BMP2 increase upon initial contact of Zn ions with HMSCs [19]. TGF-β phosphorylates smad2 and smad3 proteins by binding to TGF-β receptors. These proteins, together with smad4, lead to the proliferation of chemotaxis and early differentiation [52]. BMP2 also phosphorylates smad1, smad5, and smad8 proteins via binding to BMP2 receptors [53]. When these proteins enter the cell nucleus, genes such as DLX5, OPN, OSX, and Runx2 are transcribed for cell differentiation and proliferation [52]. On the other hand, Zn increases phosphorylated CREB through stimulation of the cAMP-PKA-CREB signaling pathway, which leads to the expression of other osteogenesis markers such as OCN, ALP, Col1, and Runx2 [54].

3.1.3. Effect of rGO on Cellular Behavior

rGO in the ZnHA-rGO nanosystem, via interacting with the surface of HMSCs, will create optimal conditions for focal adhesion to differentiate. In addition, rGO increases bone scaffold strength and cell adhesion. The addition of graphene and its derivatives to bone scaffolds increases their mechanical strength and modulus [55]. Matrix stiffness plays a crucial role in the orientation of cell differentiation by stimulating the expression of specific genes. Hence, with increasing matrix stiffness, the expression of osteogenesis genes in HMSCs increases. The relationship between matrix stiffness and HMSC differentiation can be observed in Figure 8. Accordingly, the higher the matrix stiffness, the higher the expression of osteogenesis genes [56]. rGO in the ZnHA-rGO nanosystem increases the stiffness of ECM and helps osteoblastic differentiation of HMSCs. rGO causes actin polymerization by stimulating integrin (a protein that mediates between ECM and cytoskeleton). Integrin stimulation creates a chain of connections between the Talin, Vinculin, Zyxin, Actinin, Paxillin, Parvin, and FAK proteins. FAK helps to activate RhoA and subsequently ROCK by phosphorylating RhoGEF [57]. ROCK phosphorylates MLC, which induces actin polymerization. The actin polymerization, followed by forming actin filaments attached to myosin, causes internal forces in the cytoskeleton [58] (between the nucleus and the membrane). These internal forces lead to more calcium ions entering the cell and mechanotransduction signaling events, which activate the transcription factors YAP and TAZ [59]. Besides, FAK activates the β-catenin protein by activating the PI3K-AKT pathway, which is a major transcription factor in the expression of genes involved in osteoblast proliferation [60]. Alternatively, rGO phosphorylates p130Cas by stimulating integrin and FAK, leading to Crk activation. Finally, Crk activates JNK by stimulating Dock180 and ELMO and subsequently Rac. As a result, more activity of FOXO1 can be seen, an important transcription factor in osteoblast differentiation [61]. On the other hand, Crk activity can activate GRF2, Rap1, and Raf1, and subsequently can phosphorylate MEK and ERK, and this pathway increases phosphorylated CREB [62].

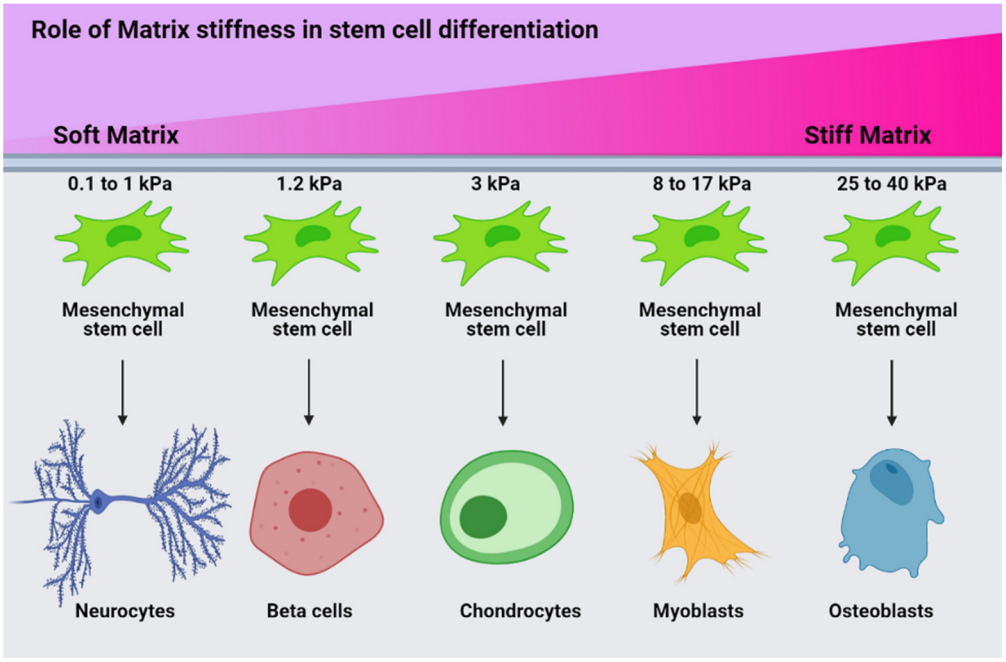

Figure 8. Schematic representation of the relationship between matrix stiffness and HMSC differentiation. Matrix stiffness significantly affects the differentiation of HMSCs; higher stiffness leads to osteogenic differentiation.

3.1.4. Synergistic Effect in ZnHA-rGO Nanosystem

As a result, not only Zn and HA increase CREB-activated transcription factor levels, but also rGO has a similar effect on upregulating CREB-related genes. Generally, Zn, HA, and rGO in this nanosystem can increase the level of transcription factors related to osteogenesis by stimulating specific signaling pathways. Since each of the HA, Zn, and rGO agents individually have positive effects on osteogenesis and cell proliferation, using a combination of these agents in a nanocomposite form helps to generate a synergistic effect on the proliferation and osteogenic differentiation of HMSCs. The synergistic effect of this nanosystem leads to the activation of important transcription factors for the expression of genes related to osteogeneses such as Smad1, Smad2, Smad3, Smad4, Smad5, Smad8, β-catenin, CREB, FOXO1, TAZ, and YAP. The synergistic influence of this nanosystem on the proliferation and osteoblastic differentiation of HMSC can be observed in the schematic presented in Figure 9.

3.2. Antibacterial Behavior

3.2.1. Effect of Hydroxyapatite on Antibacterial Behavior

The HA nanoparticles can have an antibacterial effect against both Gram-positive and Gram-negative bacteria. HA causes mechanical damage to the bacterial membrane due to its abrasive surface [63]. Electrostatic interaction between HA nanoparticles and the bacterial cell wall can lead to the entry of nanoparticles into the cytoplasm. With the entry of HA and its reformation inside the bacterium, it will cause the bacterium's death. The antibacterial efficiency of HA nanoparticles will be increased by activation of groveling and spores [63,64]. In addition, HA increases oxidative stress by affecting the amount of ROS inside and outside the cell. Oxidative stress attacks many of the cell components inside a bacterium that are needed for life [65]. Gram-positive bacteria are also less sensitive to HA nanoparticles than Gram-negative bacteria, due to differences in membrane structure.

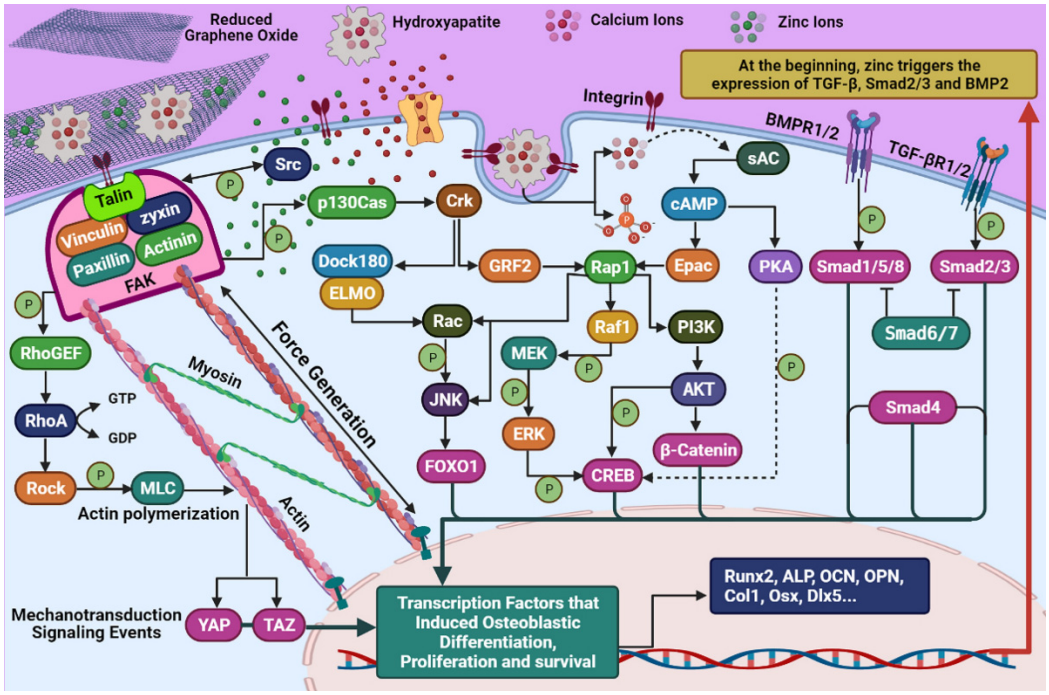

Figure 9. Schematic representation of ZnHA-rGO nanosystem interactions with MSC. The illustration shows the molecular mechanism of proliferation modulation and osteogenic differentiation of MSC by the ZnHA-rGO nanosystem through signaling pathways.

3.2.2. Effect of Zinc on Antibacterial Behavior

The ZnHA nanoparticles attack bacteria by different mechanisms. These mechanisms are divided into two categories: direct interaction of nanoparticles with bacteria and interaction of released Zn^{2+} ions with the bacterial wall and its constituents. ZnHA nanoparticles can damage the wall and membrane of bacteria and enter the bacteria through channels, damaged areas, and accumulate in the cytoplasm. Accumulation of nanoparticles within bacteria is one of the possible mechanisms in the death of bacteria by ZnHA nanoparticles [66]. However, as shown in the antibacterial test results presented in Figures 6 and 7, it has been found that Gram-positive bacteria are less sensitive to ZnHA nanoparticles than Gram-negative bacteria. The reason for this can be attributed to the greater thickness of the peptidoglycan layer in Gram-positive bacteria [67,68] in such a way that the predominant mechanism of inhibiting Gram-positive *S. aureus* bacteria by ZnHA nanoparticles can be attributed to the induction of downregulating of amino acid synthesis and dysfunction of vital bacterial enzymes [69]. Another mechanism of bacterial inhibition is related to Zn^{2+} ions released from the ZnHA-rGO nanosystem into bacteria. For example, Zn^{2+} ions can interfere with mitochondrial function or damage DNA and RNA. In addition, high concentrations of Zn^{2+} ions in bacteria may alter the three-dimensional conformation of proteins and disrupt the function of enzymes and electron transport chains [70].

3.2.3. Effect of rGO on Antibacterial Behavior

rGO and GO both have antibacterial properties. rGO, as a component of the nanocomposite, has several mechanisms to inhibit bacterial growth. The principal antibacterial mechanism of rGO for Gram-negative and -positive bacteria is cell wall mechanical damage and inhibition of cell division, respectively [71]. Antibacterial mechanisms of rGO include cell entrapment, bacterial aggregation by rGO sheet, a sharp edge-mediated cutting effect that leads to rupture of the bacterial cell wall, and oxidative stress by increasing ROS levels leading to structural damage to nucleic acids and proteins [72]. Since the three components of the nanocomposite can damage the cell wall and intracellular components of bacteria, the synergistic effect of these materials creates a higher antibacterial potential for this

nanosystem. The synergistic effect of the nanosystem compounds in the face of bacteria can be seen in a schematic presentation in Figure 10.

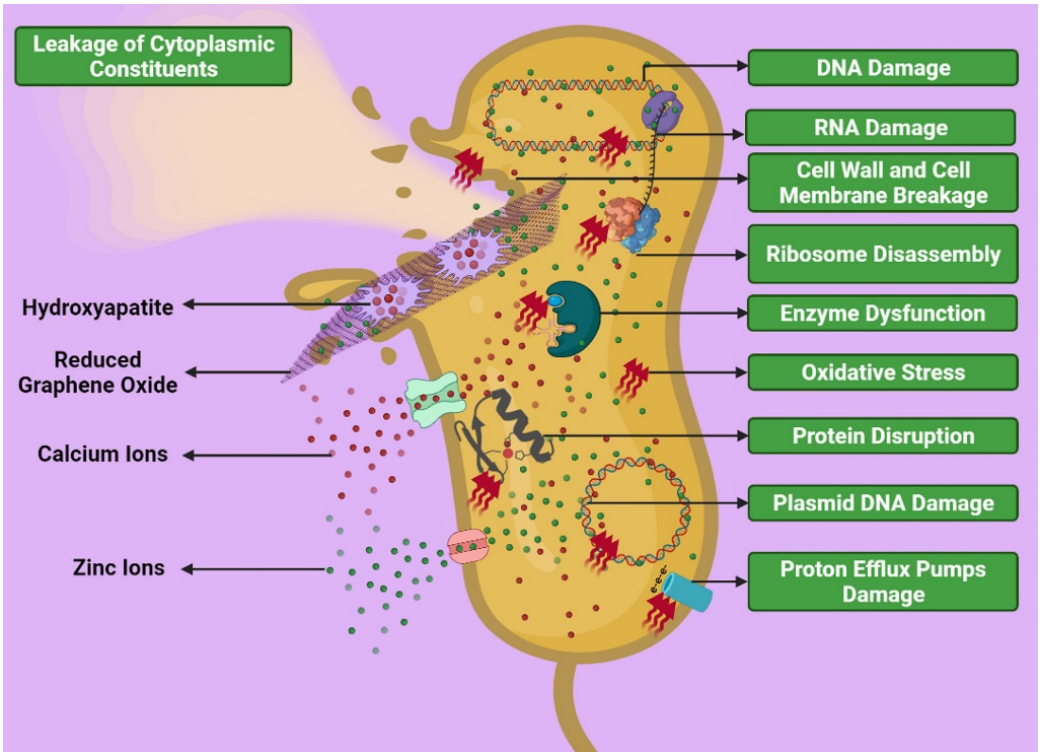

Figure 10. The possible interaction of the ZnHA-rGO nanosystem in the face of bacteria. The three components of the nanocomposite (HA, Zn^{2+}, and rGO) damage the cell wall and intracellular components of bacteria.

4. Materials and Methods

4.1. Material Preparations

Extraction of natural HA nanoparticles was performed according to the method presented in a previous study [34]. Doping Zn in HA nanoparticles and compositing it with rGO has also been described in a previous study [34].

4.2. Characterization

To study the morphology and structure of nanoparticles, TEM, XRD, and Raman spectroscopy analyses were used. Morphology of the nanopowders was analyzed using transmission electron microscopy (TEM, JEOL JEM-ARM200CFEG UHR-TEM). The XRD examination was also conducted using a single-beam, Cu Kα, λ = 1.5406 Å (PANalytical, Pro MPD model, Almelo, Netherlands). The step size and step time of XRD were considered as 0.02° and 2 s, respectively. The Raman spectra were achieved by an inVia Reflex Renishaw (Wotton-under-Edge, Gloucestershire, United Kingdom) Raman spectrometer equipped with a laser diode (λ = 785 nm, 30 mW).

4.3. Cellular Behavior

4.3.1. Cell Culture

The initial density of 10^5 MSCs/well was seeded in a culture plate containing Dulbecco's modified Eagle's medium (DMEM). Then, 10% fetal bovine serum (FBS) and 1% penicillin-streptomycin were added to the mixture. The culture media were incubated at 37 °C in a humidified atmosphere of 5% CO_2. After overnight incubation, the cells were treated with 100 μg mL^{-1} concentrations of nanoparticles. The media were replaced with fresh ones at intervals of two days.

4.3.2. Cell Viability Assessment

The proliferation of MSCs for culture media treated with nanoparticles was investigated for 7 and 14 days by MTT assay.

The MTT assay (Sigma Inc., Marlborough, MA, USA) was carried out to assess the expansion of MSCs cultured on 24 well plates. At the first step, 5 mg of MTT powder was dissolved in phosphate-buffered saline (PBS) solution. To dilute the MTT solution in the second step, 900 µL of DMEM/F12 medium was added to the solution. In the third step, 1 mL of the prepared solution was poured into each well to form the Formazan crystals and kept in dark incubation for 2 h. Then, the supernatants of the wells were removed completely, and for dissolving the prepared crystals, 1 mL of a stabilized solution (including 10% Triton x-100, 0.1 M HCl, and isopropanol) was added to each well. Finally, a microplate (Elx808, BioTek, Winooski, VT, USA) at a wavelength of 570 nm was used to read the absorbance of each well sample.

4.3.3. Alkaline Phosphatase Activity

ALP is an osteogenic marker whose activation is intensified in the bone growth duration; the expression value of ALP rises during the beginning of differentiation of MSCs [45,46]. Such an increment of ALP expression develops bone formation by nucleating calcium phosphate on ECM, causing mineralization, and acting as an essential function in osteoblast differentiation and maturation [45,46].

The HA, ZnHA, and ZnHA-rGO nanoparticles were exposed to MSCs for 7 and 14 days to assess their ALP activities. After incubation, the MSCs were washed with PBS, lysed by lysis buffer, incubated for 30 min at 37 °C, and held for 12 h at 4 °C. Afterwards, the cells were centrifuged for 10 min at 12,000 rpm. Then, the supernatant and p-nitrophenyl phosphate solution (1 to 20) were mixed and incubated for 1 h at 25 °C. The ALP activity was determined utilizing the fluorescence microscope system (Cytation 5, BioTek, Winooski, VT, USA) at a wavelength of 405 nm.

4.4. Antibacterial Activity

To assess antibacterial activities, the samples were tested using both *E. coli* and *S. aureus* bacteria, because these are the two most common bacteria in any hospital environment that can cause bacterial infection. Moreover, bacteria belonging to both groups were selected; Gram-positive (*E. coli*) and Gram-negative (*S. aureus*).

4.4.1. Cell Viability Assessment

The nanoparticles were dispersed in deionized (DI) water with concentration of 100 µg mL^{-1}. In addition, dilution 10^6 CFU/mL of bacteria were incubated with dispersed nanoparticles in DI water at 37 °C under 150 rpm stirring speed for up to 6 h. Bacterial samples in DI water without nanoparticles were considered as the control. Eventually, 100 µL of each sample was spread onto LB plates after each 4 h of time interval and left to grow for 12 h at 37 °C. Colonies were counted and compared with those of the control samples to determine the total viable count and percentage of the non-viable cells.

4.4.2. Disk Diffusion Method

The disk diffusion test was carried out by pouring lysogeny broth and brain heart infusion agar into Petri dishes. The nanoparticles (50 mg) suspended in ethanol were applied to sterilized filter paper disks (6 mm in diameter). Bacteria suspension (100 µL) was spread uniformly on the surface of solidified nutrient agar, followed by placing sterilized disk specimens onto the agar dishes. Finally, samples were placed in an incubator with a humidified atmosphere of 5% CO_2 and 95% air for 18 h at 37 °C. All disk diffusion tests were performed in triplicate, and the diameters (mm) of the inhibition zone were measured after incubation.

5. Conclusions

In this work, HA nanoparticles extracted from bovine cortical bone were doped with Zn by mechanical alloying. The ZnHA nanoparticles were also composited with rGO by photochemical reduction. The microstructural studies confirmed the hexagonal crystal structure for HA and ZnHA nanoparticles. The influence of HA nanoparticles on stem cell behavior revealed no toxic effect, and significantly improved cell proliferation and alkaline phosphatase activity, and that Zn and rGO have a synergistic effect on these behaviors. The antibacterial test results showed that HA nanoparticles have antibacterial function against Gram-negative (E. coli) and Gram-positive (*S. aureus*) bacteria. The antibacterial activity of HA nanoparticles was significantly increased by Zn doping such that the bacterial cell loss raised to 3-fold in 12 h. Finally, rGO also had a positive effect on increasing the antibacterial activity of the ZnHA nanoparticles.

Author Contributions: Conceptualization, H.M.-G.; methodology, H.M.-G., A.F. and P.K.-A.; software, E.M.-T. and P.K.-A.; validation, Y.B.-K.; formal analysis, H.M.-G., A.F. and M.K.; investigation, H.M.-G., A.F., M.K., P.K.-A. and E.M.-T.; resources, Y.O., J.B. and Y.B.-K.; data curation, Y.B.-K.; writing—original draft preparation, H.M.-G.; writing—review and editing, M.H.S., B.K., P.K.-A., Y.B.-K., A.P.K. and K.A.; visualization, M.H.S., B.K., Y.B.-K., A.P.K. and K.A.; supervision, K.A.; project administration, H.M.-G. and K.A.; funding acquisition, A.P.K. All authors have read and agreed to the published version of the manuscript.

Funding: The work was supported by a grant from the Singapore Ministry of Education Tier 2 (MOE-T2EP30120-0016) to A.P.K. A.P.K. is also supported by the National Medical Research Council of Singapore and the Singapore Ministry of Education under its Research Centers of Excellence initiative to the Cancer Science Institute of Singapore, National University of Singapore.

Institutional Review Board Statement: Not applicable.

Informed Consent Statement: Not applicable.

Data Availability Statement: All data generated or analyzed during this study are included in the present article.

Conflicts of Interest: The authors declare no conflict of interest.

References

1. Ribeiro, M.; Monteiro, F.; Ferraz, M.P. Infection of orthopedic implants with emphasis on bacterial adhesion process and techniques used in studying bacterial-material interactions. *Biomatter* **2012**, *2*, 176–194. [CrossRef] [PubMed]
2. Arciola, C.R.; Campoccia, D.; Montanaro, L. Implant infections: Adhesion, biofilm formation and immune evasion. *Nat. Rev. Genet.* **2018**, *16*, 397–409. [CrossRef] [PubMed]
3. Masters, E.A.; Trombetta, R.P.; de Mesy Bentley, K.L.; Boyce, B.F.; Gill, A.L.; Gill, S.R.; Nishitani, K.; Ishikawa, M.; Morita, Y.; Ito, H.; et al. Evolving concepts in bone infection: Redefining "biofilm", "acute vs. chronic osteomyelitis", "the immune proteome" and "local antibiotic therapy". *Bone Res.* **2019**, *15*, 1–8. [CrossRef]
4. Johnson, C.; García, A.J. Scaffold-based anti-infection strategies in bone repair. *Ann. Biomed. Eng.* **2014**, *43*, 515–528. [CrossRef] [PubMed]
5. Vallet-Regí, M.; Lozano, D.; González, B.; Izquierdo-Barba, I. Biomaterials against bone infection. *Adv. Healthc. Mater.* **2020**, *9*, 2000310. [CrossRef]
6. Khalili, V.; Khalil-Allafi, J.; Maleki-Ghaleh, H. Characterisation of HA–Si composite coatings on NiTi for biomedical applications. *Surf. Eng.* **2013**, *30*, 212–217. [CrossRef]
7. Keikhosravani, P.; Maleki-Ghaleh, H.; Khosrowshahi, A.K.; Bodaghi, M.; Dargahi, Z.; Kavanlouei, M.; Khademi-Azandehi, P.; Fallah, A.; Beygi-Khosrowshahi, Y.; Siadati, M.H. Bioactivity and antibacterial behaviors of nanostructured lithium-doped hydroxyapatite for bone scaffold application. *Int. J. Mol. Sci.* **2021**, *22*, 9214. [CrossRef]
8. Khosrowshahi, A.K.; Khoshfetrat, A.B.; Khosrowshahi, Y.B.; Maleki-Ghaleh, H. Cobalt content modulates characteristics and osteogenic properties of cobalt-containing hydroxyapatite in in-vitro milieu. *Mater. Today Commun.* **2021**, *27*, 102392. [CrossRef]
9. Chocholata, P.; Kulda, V.; Babuska, V. Fabrication of scaffolds for bone-tissue regeneration. *Materials* **2019**, *12*, 568. [CrossRef]
10. Maleki-Ghaleh, H.; Aghaie, E.; Nadernezhad, A.; Zargarzadeh, M.; Khakzad, A.; Shakeri, M.S.; Khosrowshahi, Y.B.; Siadati, M.H. Influence of Fe_3O_4 nanoparticles in hydroxyapatite scaffolds on proliferation of primary human fibroblast cells. *J. Mater. Eng. Perform.* **2016**, *25*, 2331–2339. [CrossRef]
11. Khan, W.S.; Rayan, F.; Dhinsa, B.S.; Marsh, D. An osteoconductive, osteoinductive, and osteogenic tissue-engineered product for trauma and orthopaedic surgery: How far are we? *Stem Cells Int.* **2011**, *2012*, 1–7. [CrossRef]

12. Wang, P.; Zhao, L.; Liu, J.; Weir, M.D.; Zhou, X.; Xu, H.H.K. Bone tissue engineering via nanostructured calcium phosphate biomaterials and stem cells. *Bone Res.* **2014**, *2*, 14017. [CrossRef]
13. Katti, K.S.; Jasuja, H.; Kar, S.; Katti, D.R. Nanostructured biomaterials for in vitro models of bone metastasis cancer. *Curr. Opin. Biomed. Eng.* **2020**, *17*, 100254. [CrossRef]
14. Luo, J.; Mamat, B.; Yue, Z.; Zhang, N.; Xu, X.; Li, Y.; Su, Z.; Ma, C.; Zang, F.; Wang, Y. Multi-metal ions doped hydroxyapatite coatings via electrochemical methods for antibacterial and osteogenesis. *Colloid Interface Sci. Commun.* **2021**, *43*, 100435. [CrossRef]
15. Li, M.; Xiong, P.; Yan, F.; Li, S.; Ren, C.; Yin, Z.; Li, A.; Li, H.; Ji, X.; Zheng, Y.; et al. An overview of graphene-based hydroxyapatite composites for orthopedic applications. *Bioact. Mater.* **2018**, *3*, 1–18. [CrossRef]
16. Pasquet, J.; Chevalier, Y.; Pelletier, J.; Couval, E.; Bouvier, D.; Bolzinger, M.-A. The contribution of zinc ions to the antimicrobial activity of zinc oxide. *Colloids Surf. A Physicochem. Eng. Asp.* **2014**, *457*, 263–274. [CrossRef]
17. Predoi, D.; Iconaru, S.L.; Predoi, M.V.; Motelica-Heino, M.; Guegan, R.; Buton, N. Evaluation of antibacterial activity of zinc-doped hydroxyapatite colloids and dispersion stability using ultrasounds. *Nanomaterials* **2019**, *9*, 515. [CrossRef]
18. Tang, Y.; Rajendran, P.; Veeraraghavan, V.P.; Hussain, S.; Balakrishna, J.P.; Chinnathambi, A.; Alharbi, S.A.; Alahmadi, T.A.; Rengarajan, T.; Mohan, S.K. Osteogenic differentiation and mineralization potential of zinc oxide nanoparticles from *Scutellaria baicalensis* on human osteoblast-like MG-63 cells. *Mater. Sci. Eng. C* **2020**, *119*, 111656. [CrossRef]
19. Yu, J.; Xu, L.; Li, K.; Xie, N.; Xi, Y.; Wang, Y.; Zheng, X.; Chen, X.; Wang, M.; Ye, X. Zinc-modified calcium silicate coatings promote osteogenic differentiation through TGF-β/Smad pathway and osseointegration in osteopenic rabbits. *Sci. Rep.* **2017**, *7*, 1–13. [CrossRef]
20. Moonga, B.S.; Dempster, D.W. Zinc is a potent inhibitor of osteoclastic bone resorption in vitro. *J. Bone Miner. Res.* **2009**, *10*, 453–457. [CrossRef]
21. Alcantara, E.H.; Lomeda, R.-A.R.; Feldmann, J.; Nixon, G.F.; Beattie, J.H.; Kwun, I.-S. Zinc deprivation inhibits extracellular matrix calcification through decreased synthesis of matrix proteins in osteoblasts. *Mol. Nutr. Food Res.* **2011**, *55*, 1552–1560. [CrossRef] [PubMed]
22. Fu, X.; Li, Y.; Huang, T.; Yu, Z.; Ma, K.; Yang, M.; Liu, Q.; Pan, H.; Wang, H.; Wang, J.; et al. Runx2/Osterix and zinc uptake synergize to orchestrate osteogenic differentiation and citrate containing bone apatite formation. *Adv. Sci.* **2018**, *5*, 1700755. [CrossRef]
23. Chen, C.T.; Shih, Y.R.; Kuo, T.K.; Lee, O.K.; Wei, Y.H. Coordinated changes of mitochondrial biogenesis and antioxidant enzymes during osteogenic differentiation of human mesenchymal stem cells. *Stem Cells* **2008**, *26*, 960–968. [CrossRef] [PubMed]
24. Huang, T.; Liu, R.; Fu, X.; Yao, D.; Yang, M.; Liu, Q.; Lu, W.W.; Wu, C.; Guan, M. Aging reduces an ERRalpha-directed mitochondrial glutaminase expression suppressing glutamine anaplerosis and osteogenic differentiation of mesenchymal stem cells. *Stem Cells* **2017**, *35*, 411–424. [CrossRef]
25. Granchi, D.; Baldini, N.; Ulivieri, F.M.; Caudarella, R. Role of citrate in pathophysiology and medical management of bone diseases. *Nutrients* **2019**, *11*, 2576. [CrossRef]
26. Costello, L.C.; Franklin, R.B.; Liu, Y.; Kennedy, M. Zinc causes a shift toward citrate at equilibrium of the m-aconitase reaction of prostate mitochondria. *J. Inorg. Biochem.* **2000**, *78*, 161–165. [CrossRef]
27. Shareena, T.P.D.; McShan, D.; DasMahapatra, A.K.; Tchounwou, P.B. A review on graphene-based nanomaterials in biomedical applications and risks in environment and health. *Nano-Micro Lett.* **2018**, *10*, 1–34. [CrossRef]
28. Tadyszak, K.; Wychowaniec, J.K.; Litowczenko, J. Biomedical applications of graphene-based structures. *Nanomaterials* **2018**, *8*, 944. [CrossRef]
29. Kang, M.S.; Jeong, S.J.; Lee, S.H.; Kim, B.; Hong, S.W.; Lee, J.H.; Han, D.-W. Reduced graphene oxide coating enhances osteogenic differentiation of human mesenchymal stem cells on Ti surfaces. *Biomater. Res.* **2021**, *25*, 1–9. [CrossRef] [PubMed]
30. Qiu, J.; Geng, H.; Wang, D.; Qian, S.; Zhu, H.; Qiao, Y.; Qian, W.; Liu, X. Layer-number dependent antibacterial and osteogenic behaviors of graphene oxide electrophoretic deposited on titanium. *ACS Appl. Mater. Interfaces* **2017**, *9*, 12253–12263. [CrossRef]
31. Liu, S.; Zeng, T.H.; Hofmann, M.; Burcombe, E.; Wei, J.; Jiang, R.; Kong, J.; Chen, Y. Antibacterial activity of graphite, graphite oxide, graphene oxide, and reduced graphene oxide: Membrane and oxidative stress. *ACS Nano* **2011**, *5*, 6971–6980. [CrossRef]
32. Lee, J.H.; Shin, Y.C.; Jin, O.S.; Kang, S.H.; Hwang, Y.-S.; Park, J.-C.; Hong, S.W.; Han, D.-W. Reduced graphene oxide-coated hydroxyapatite composites stimulate spontaneous osteogenic differentiation of human mesenchymal stem cells. *Nanoscale* **2015**, *7*, 11642–11651. [CrossRef]
33. Hermenean, A.; Dinescu, S.; Ionita, M.; Costache, M. The impact of graphene oxide on bone regeneration therapies. *Adv. Technol.* **2016**. [CrossRef]
34. Maleki-Ghaleh, H.; Siadati, M.H.; Fallah, A.; Zarrabi, A.; Afghah, F.; Koc, B.; Abdolahinia, E.D.; Omidi, Y.; Barar, J.; Akbari-Fakhrabadi, A.; et al. Effect of zinc-doped hydroxyapatite/graphene nanocomposite on the physicochemical properties and osteogenesis differentiation of 3D-printed polycaprolactone scaffolds for bone tissue engineering. *Chem. Eng. J.* **2021**, *426*, 131321. [CrossRef]
35. Maleki-Ghaleh, H.; Khalil-Allafi, J. Effect of hydroxyapatite-titanium-MWCNTs composite coating fabricated by electrophoretic deposition on corrosion and cellular behavior of NiTi alloy. *Mater. Corros.* **2019**, *70*, 2128–2138. [CrossRef]
36. Maleki-Ghaleh, H.; Khalili, V.; Khalil-Allafi, J.; Javidi, M.M. Hydroxyapatite coating on NiTi shape memory alloy by electrophoretic deposition process. *Surf. Coat. Technol.* **2012**, *208*, 57–63. [CrossRef]

37. Maleki-Ghaleh, H.; Khalil-Allafi, J.; Horandghadim, N.; Keikhosravani, P.; Hosseini, M.G. Structural characterization, mechanical, and electrochemical studies of hydroxyapatite-titanium composite coating fabricated using electrophoretic deposition and reaction bonding process. *J. Biomed. Mater. Res. Part B Appl. Biomaterials.* **2020**, *108*, 2119–2130. [CrossRef]
38. Khalili, V.; Khalil-Allafi, J.; Maleki-Ghaleh, H.; Paulsen, A.; Frenzel, J.; Eggeler, G. The influence of Si as reactive bonding agent in the electrophoretic coatings of HA-Si-MWCNTs on NiTi alloys. *J. Mater. Eng. Perform.* **2015**, *25*, 390–400. [CrossRef]
39. Saleem, H.; Haneef, M.; Abbasi, H.Y. Synthesis route of reduced graphene oxide via thermal reduction of chemically exfoliated graphene oxide. *Mater. Chem. Phys.* **2018**, *204*, 1–7. [CrossRef]
40. Guerra-López, J.R.; Echeverría, G.A.; Güida, J.A.; Viña, R.; Punte, G. Synthetic hydroxyapatites doped with Zn (II) studied by X-ray diffraction, infrared, Raman and thermal analysis. *J. Phys. Chem. Solids* **2015**, *1*, 57–65. [CrossRef]
41. Yuan, Q.; Wu, J.; Qin, C.; Xu, A.; Zhang, Z.; Lin, Y.; Chen, Z.; Lin, S.; Yuan, Z.; Ren, X.; et al. One-pot synthesis and characterization of Zn-doped hydroxyapatite nanocomposites. *Mater. Chem. Phys.* **2017**, *199*, 122–130. [CrossRef]
42. Jastrzębski, W.; Sitarz, M.; Rokita, M.; Bułat, K. Infrared spectroscopy of different phosphates structures. *Spectrochim. Acta Mol. Biomol. Spectrosc.* **2011**, *79*, 722–727. [CrossRef]
43. Alam, M.K.; Rahman, M.M.; Elzwawy, A.; Torati, S.R.; Islam, M.S.; Todo, M.; Asiri, A.M.; Kim, D.; Kim, C. Highly sensitive and selective detection of Bis-phenol A based on hydroxyapatite decorated reduced graphene oxide nanocomposites. *Electrochim. Acta.* **2017**, *241*, 353–361. [CrossRef]
44. Maleki-Ghaleh, H.; Khalil-Allafi, J.; Keikhosravani, P.; Etminanfar, M.R.; Behnamian, Y. Effect of nano-zirconia on microstructure and biological behavior of hydroxyapatite-based bone scaffolds. *J. Mater. Eng. Perform.* **2020**, *29*, 4412–4420. [CrossRef]
45. Sharma, U.; Pal, D.; Prasad, R. Alkaline phosphatase: An overview. *Indian J. Clin. Biochem.* **2014**, *29*, 269–278. [CrossRef]
46. Blair, H.C.; Larrouture, Q.C.; Li, Y.; Lin, H.; Beer-Stoltz, D.; Liu, L.; Tuan, R.S.; Robinson, L.J.; Schlesinger, P.H.; Nelson, D.J. Osteoblast differentiation and bone matrix formation in vivo and in vitro. *Tissue Eng. Rev.* **2017**, *23*, 268–280. [CrossRef] [PubMed]
47. Xu, D.; Wan, Y.; Li, Z.; Wang, C.; Zou, Q.; Du, C.; Wang, Y. Tailorable hierarchical structures of biomimetic hydroxyapatite micro/nano particles promoting endocytosis and osteogenic differentiation of stem cells. *Biomater. Sci.* **2020**, *8*, 3286–3300. [CrossRef] [PubMed]
48. Yu, X.; Zhang, Q.; Zhao, Y.; Schwarz, B.J.; Stallone, J.N.; Heaps, C.L.; Han, G. Activation of G protein-coupled estrogen receptor 1 induces coronary artery relaxation via Epac/Rap1-mediated inhibition of RhoA/Rho kinase pathway in parallel with PKA. *PLoS ONE* **2017**, *12*, e0173085. [CrossRef]
49. Heiser, J.H.; Schuwald, A.M.; Sillani, G.; Ye, L.; Müller, W.E.; Leuner, K. TRPC 6 channel-mediated neurite outgrowth in PC 12 cells and hippocampal neurons involves activation of RAS/MEK/ERK, PI 3K, and CAMKIV signaling. *J. Neurochem.* **2013**, *127*, 303–313. [CrossRef]
50. Amarasekara, D.; Kim, S.; Rho, J. Regulation of osteoblast differentiation by cytokine networks. *Int. J. Mol. Sci.* **2021**, *22*, 2851. [CrossRef]
51. O'Connor, J.P.; Kanjilal, D.; Teitelbaum, M.; Lin, S.S.; Cottrell, J.A. Zinc as a therapeutic agent in bone regeneration. *Materials* **2020**, *13*, 2211. [CrossRef]
52. Wu, M.; Chen, G.; Li, Y.P. TGF-β and BMP signaling in osteoblast, skeletal development, and bone formation, homeostasis and disease. *Bone Res.* **2016**, *4*, 1–21. [CrossRef]
53. Mitsui, Y.; Hirata, H.; Arichi, N.; Hiraki, M.; Yasumoto, H.; Chang, I.; Fukuhara, S.; Yamamura, S.; Shahryari, V.; Deng, G.; et al. Inactivation of bone morphogenetic protein 2 may predict clinical outcome and poor overall survival for renal cell carcinoma through epigenetic pathways. *Oncotarget* **2015**, *6*, 9577–9591. [CrossRef]
54. Park, K.H.; Choi, Y.; Yoon, D.S.; Lee, K.M.; Kim, D.; Lee, J.W. Zinc promotes osteoblast differentiation in human mesenchymal stem cells via activation of the cAMP-PKA-CREB signaling pathway. *Stem Cells Dev.* **2018**, *27*, 1125–1135. [CrossRef]
55. Peng, S.; Feng, P.; Wu, P.; Huang, W.; Yang, Y.; Guo, W.; Gao, C.; Shuai, C. Graphene oxide as an interface phase between polyetheretherketone and hydroxyapatite for tissue engineering scaffolds. *Sci. Rep.* **2017**, *7*, srep46604. [CrossRef]
56. Han, S.; Kim, J.; Lee, G.; Kim, D. Mechanical properties of materials for stem cell differentiation. *Adv. Biosyst.* **2020**, *4*, e2000247. [CrossRef]
57. Stutchbury, B.; Atherton, P.; Tsang, R.; Wang, D.-Y.; Ballestrem, C. Distinct focal adhesion protein modules control different aspects of mechanotransduction. *J. Cell Sci.* **2017**, *130*, 1612–1624. [CrossRef]
58. Footer, M.J.; Kerssemakers, J.W.J.; Theriot, J.; Dogterom, M. Direct measurement of force generation by actin filament polymerization using an optical trap. *Proc. Natl. Acad. Sci. USA* **2007**, *104*, 2181–2186. [CrossRef]
59. Park, J.H.; Shin, J.E.; Park, H.W. The role of hippo pathway in cancer stem cell biology. *Mol. Cells* **2018**, *41*, 83–92. [CrossRef] [PubMed]
60. Yang, C.-M.; Ji, S.; Li, Y.; Fu, L.-Y.; Jiang, T.; Meng, F.-D. β-Catenin promotes cell proliferation, migration, and invasion but induces apoptosis in renal cell carcinoma. *Oncotargets Ther.* **2017**, *10*, 711–724. [CrossRef] [PubMed]
61. Halim, A.; Liu, L.; Ariyanti, A.D.; Ju, Y.; Luo, Q.; Song, G. Low-dose suspended graphene oxide nanosheets induce antioxidant response and osteogenic differentiation of bone marrow-derived mesenchymal stem cells via JNK-dependent FoxO1 activation. *J. Mater. Chem. B* **2019**, *7*, 5998–6009. [CrossRef]
62. Li, X.; Guo, C.; Li, Y.; Li, L.; Wang, Y.; Zhang, Y.; Li, Y.; Chen, Y.; Liu, W.; Gao, L. Ketamine administered pregnant rats impair learning and memory in offspring via the CREB pathway. *Oncotarget* **2017**, *8*, 32433–32449. [CrossRef]

63. Ragab, H.S.; Ibrahim, F.A.; Abdallah, F.; Al-Ghamdi, A.A.; El-Tantawy, F.; Yakuphanoglu, F. Synthesis and in vitro antibacterial properties of hydroxyapatite nanoparticles. *IOSR J. Pharm. Biol. Sci.* **2014**, *9*, 77–85. [CrossRef]
64. Sadat-Shojai, M.; Khorasani, M.T.; Dinpanah-Khoshdargi, E.; Jamshidi, A. Synthesis methods for nanosized hydroxyapatite with diverse structures. *Acta Biomater.* **2013**, *9*, 7591–7621. [CrossRef]
65. Wang, M.; Li, M.; Wang, Y.; Shao, Y.; Zhu, Y.; Yang, S. Efficient antibacterial activity of hydroxyapatite through ROS generation motivated by trace Mn(iii) coupled H vacancies. *J. Mater. Chem. B* **2021**, *9*, 3401–3411. [CrossRef] [PubMed]
66. Dimapilis, E.A.S.; Hsu, C.-S.; Mendoza, R.M.O.; Lu, M.-C. Zinc oxide nanoparticles for water disinfection. *Sustain. Environ. Res.* **2017**, *28*, 47–56. [CrossRef]
67. Rutherford, D.; Jíra, J.; Kolářová, K.; Matolínová, I.; Mičová, J.; Remeš, Z.; Rezek, B. Growth inhibition of gram-positive and gram-negative bacteria by zinc oxide hedgehog particles. *Int. J. Nanomed.* **2021**, *16*, 3541–3554. [CrossRef]
68. Sinha, R.; Karan, R.; Sinha, A.; Khare, S. Interaction and nanotoxic effect of ZnO and Ag nanoparticles on mesophilic and halophilic bacterial cells. *Bioresour. Technol.* **2011**, *102*, 1516–1520. [CrossRef] [PubMed]
69. Kadiyala, U.; Turali-Emre, E.S.; Bahng, J.H.; Kotov, N.A.; Vanepps, J.S. Unexpected insights into antibacterial activity of zinc oxide nanoparticles against methicillin resistant *Staphylococcus aureus* (MRSA). *Nanoscale* **2018**, *10*, 4927–4939. [CrossRef] [PubMed]
70. Yusof, H.M.; Mohamad, R.; Zaidan, U.H.; Rahman, N.A.A. Microbial synthesis of zinc oxide nanoparticles and their potential application as an antimicrobial agent and a feed supplement in animal industry: A review. *J. Anim. Sci. Biotechnol.* **2019**, *10*, 1–22. [CrossRef]
71. Pulingam, T.; Thong, K.L.; Ali, E.; Appaturi, J.N.; Dinshaw, I.J.; Ong, Z.Y.; Leo, B.F. Graphene oxide exhibits differential mechanistic action towards Gram-positive and Gram-negative bacteria. *Colloids Surf. Biointerfaces* **2019**, *181*, 6–15. [CrossRef] [PubMed]
72. Xia, M.-Y.; Xie, Y.; Yu, C.-H.; Chen, G.-Y.; Li, Y.-H.; Zhang, T.; Peng, Q. Graphene-based nanomaterials: The promising active agents for antibiotics-independent antibacterial applications. *J. Control. Release* **2019**, *307*, 16–31. [CrossRef] [PubMed]